Letter | Editors' Suggestion

Emulating moiré materials with quasiperiodic circuit quantum electrodynamics

T. Herrig [1,2,*] C. Koliofoti [1] J. H. Pixley [3,4] E. J. König [5,6] and R.-P. Riwar [1]

[1] *Peter Grünberg Institute, Theoretical Nanoelectronics, Forschungszentrum Jülich, D-52425 Jülich, Germany*

[2] *Institute for Quantum Materials and Technology, Karlsruhe Institute of Technology, 76131 Karlsruhe, Germany*

[3] *Department of Physics and Astronomy, Center for Materials Theory, Rutgers University, Piscataway, New Jersey 08854, USA*

[4] *Center for Computational Quantum Physics, Flatiron Institute, 162 5th Avenue, New York, NY 10010, USA*

[5] *Max-Planck Institute for Solid State Research, 70569 Stuttgart, Germany*

[6] *Department of Physics, University of Wisconsin-Madison, Madison, Wisconsin 53706, USA*

(Received 25 January 2024; revised 22 January 2025; accepted 28 March 2025; published 6 May 2025)

Topological band structures interfering with moiré superstructures give rise to a plethora of emergent phenomena, which are pivotal for correlated insulating and superconducting states of twisttronics materials. While quasiperiodicity was up to now a notion mostly reserved for solid-state materials and cold atoms, we here demonstrate the capacity of conventional superconducting circuits to emulate moiré physics in charge space. With two examples, we show that Hofstadter's butterfly and the magic-angle effect are directly visible in spectroscopic transport measurements. Importantly, these features survive in the presence of harmonic trapping potentials due to parasitic linear capacitances. Our proposed platform benefits from unprecedented tuning capabilities and opens the door to probe incommensurate physics in virtually any spatial dimension.

DOI: 10.1103/PhysRevB.111.L201104

Introduction. Emulating quantum condensed matter systems has emerged as an exciting interdisciplinary frontier that hopes to utilize novel phenomena in solid state systems for technological applications in a range of engineered devices. The available emulator platforms continue to grow and currently range from acoustic and photonic metamaterials to arrays of microwave resonators to circuit quantum electrodynamics (cQED) devices [1–21]. Several tight-binding models have now been realized with a variety of geometries and structures, e.g., exhibiting a band structure with nontrivial topology [22] and higher-order topology [23,24] or emulated electrons hopping on curved space [25], as well as many-body emulators using ultracold atoms [26,27] and superconducting quantum processors [28].

With the discovery of moiré materials in twisted and stacked van der Waals heterostructures composed of graphene mulitlayers [30], transition metal dichalgonides [31], and cuprate superconductors [32], it is a timely question to understand how to generalize currently available quantum emulators to include moiré patterns. In this context, it has been understood that these patterns can be implemented by quasiperiodic potentials [33–35] which are either applied externally or arise due to lattice mismatch. This motivated several propositions of ultracold atom emulators to realize the magic-angle effect [33,36–41]. More recently, incommensurate effects have taken center stage with the culmination of experimental observations of twisted-graphene quasicrystals [42,43]. Nonetheless, experiments remain quite challenging due to incorporating specific types of optical lattices to ensure the combined presence of Dirac points and quasiperiodic

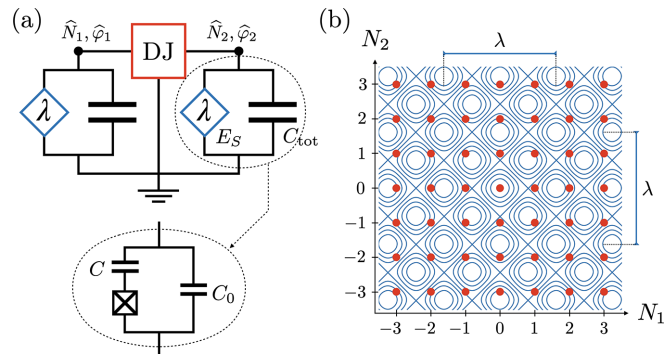

FIG. 1. Quantum circuit emulating quasiperiodicity in the space of transported charges. (a) 2D-system circuit with a three-terminal Dirac junction (DJ). The two contacts 1 and 2 are connected to ground via identical quasiperiodic nonlinear capacitors [29] with quasiperiodicity parameter λ, and stray capacitances $C_{\rm tot}$. The quasiperiodic circuit element is implemented with an auxiliary transmon (inset), where $C_{\rm tot} = C + C_0$ and $\lambda = C/C_{\rm tot}$. (b) This specific circuit provides a platform to emulate the magic-angle effect in a spin-orbit-coupled tight-binding model in a quasiperiodic potential on the square lattice. The red dots mark the discrete eigenvalues of the charge states on the two nodes, N_1 and N_2, forming the tight-binding lattice. The blue contour plot depicts the quasiperiodic potential (with periodicity λ). For nonrational λ, the potential is incommensurable with respect to the quantized charges $N_{1,2}$.

*Contact author: t-herrig@web.de

potentials. Superconducting circuits have recently emerged as a promising platform to perform band engineering within transport (instead of lattice) degrees of freedom. Beyond the obvious connection to the above solid state context, band engineering in circuits is an important topic in its own right, as it might lead to circuit hardware with significantly increased stability with respect to external noise [19] or allow for on-demand tailoring of current-phase relationships [44], which may lead to additional types of flux qubits [45].

In this Letter, we show that the conventional toolbox of cQED (i.e., nontopological Josephson junctions, capacitances, and inductances) allows us to create and measure moiré effects in the transport degrees of freedom of a quantum circuit (see Fig. 1). While we explicitly illustrate the principle with the emulation of an analog Hofstadter butterfly (HB) [56] and the magic-angle effect, note that our approach harbors the potential to effectively realize the physics of virtually any dimension [4,17] since the lattice is defined in the number of transported charges instead of the actual position space. Moreover, the generation of a nontrivial band structure occurs in a circuit element distinct from the one giving rise to the quasiperiodic potential, allowing for an exceptional degree of tunability. In particular, there exists the possibility of probing an array of devices with different electrostatic properties on the same chip or even an *in situ* control of the quasiperiodicity parameter by tuning the circuit capacitances [46]. Finally, the proposed circuits implement single-particle physics only. While, beyond doubt, the correlated many-body phases of twisted magic-angle samples are of exceptional excitement, they also wash out and bury interesting single-particle physics, including (multi)fractal features [33,47] occurring when the twist angle is incommensurate.

Note that our work builds on recently proposed quasiperiodic capacitive elements [29] introduced as a blueprint to realize cQED emulators of models for quasiperiodic Anderson localization. The presence of parasitic linear capacitances, however, prevented an explicit link between these fields to be made. Note, importantly, that parasitic capacitances lead to a harmonic trapping potential, similar to the harmonic trapping potential conventionally used in cold atom experiments, such that this represents an issue transcending the specific circuit context. The magic-angle effect, in particular, arises from a regular Dirac material with a quasiperiodic potential essentially as an incommensurate "copy-pasting" of the Dirac cone within the Brillouin zone (thus shrinking the latter) and coherent coupling of the copies. A harmonic trap fully destroys translational invariance, which is required for the existence of the Brillouin zone to begin with. That and the fact that harmonic potentials cannot be treated perturbatively (as such a potential by definition diverges away from the origin) makes it a highly nontrivial question to which degree the magic-angle transition is still observable in their presence. Therefore, a central point of our endeavor concerns the impact of said parasitic capacitances and thus of harmonic trapping potentials in general. As we explicitly demonstrate here, the known features in the density of states for both Hofstadter's butterfly and magic-angle effect in the absence of harmonic traps have a one-to-one correspondence in the density of states with traps. This makes the observation of these features amenable to standard ac spectroscopy tools, readily available in quantum circuit hardware. Furthermore, given the omnipresence of harmonic traps in other physical platforms, this surprising result is relevant beyond the here-considered quantum circuit context.

Quasiperiodic circuit QED. In our earlier work [29], we introduced the quasiperiodic nonlinear capacitor (QPNC) as a circuit element realizing an energy contribution of the form

$$\widehat{H}_{\mathrm{QPNC}} = -E_S \cos(2\pi\lambda\widehat{N}) + 2E_C\widehat{N}^2, \tag{1}$$

where $\widehat{N}$ is the number of Cooper pairs separated across the capacitor. This element can be realized with conventional superconducting materials. The nonlinear term is obtained by an approach akin to the Born-Oppenheimer approximation [48] and arises from a capacitively coupled auxiliary transmon [29] with fast degrees of freedom [see also inset in Fig. 1(a)], where E_S corresponds to the quantum phase slip amplitude within the transmon [49]. Note that for our purposes, we do *not* have to imply the strict transmon regime of $E_{JT} \gg E_{CT}$ but instead we consider only a much more relaxed regime where the energy scales of the auxiliary transmon of the QPNC to be of a similar order of magnitude $E_{JT} \sim E_{CT}$ [48]. The energy scale E_S can be controlled in a time-dependent fashion by tuning the critical current of the transmon's Josephson junction. The quasiperiodicity parameter λ corresponds to the ratio of the capacitive coupling of the transmon, C, with respect to the total capacitance, C_{tot}. The latter defines the charging energy $E_C = 2e^2/C_{\mathrm{tot}}$ of the accompanying (parasitic) linear capacitance. Therefore, λ is, in general, a real, incommensurate parameter and renders the charging energy quasiperiodic with respect to the discrete charge observable $\widehat{N}$. In Ref. [29], we explored the tunability of the parameter λ and the energy scales E_S and E_C and showed, in particular, how to tune the device into the regime of interest where the nonlinear capacitance ($\sim E_S$) is dominant compared to the linear capacitance ($\sim E_C$). Since the energy term of the latter has no upper bound but is instead characterized by its (constant) curvature, it is meaningful to demand the former to have a larger curvature to be dominant. This logic gives us the relation $\lambda^2 E_S > E_C$. This can be achieved by means of engineering effective attractive interactions [50,51], i.e., a negative capacitance. There are various ways to realize this effect, which are ultimately all rooted in the same principle: one needs to engineer an interaction yielding an energy term which has a negative second derivative (i.e., negative curvature) with respect to the charge. This principle has been pioneered and experimentally verified in quantum dots coupled to polarizers [50–52]. In Ref. [29], we generalized the polarizer principle to apply to cQED charge islands. Since λ depends (only) on capacitances, measuring features as a function of λ is a little more sophisticated. One could either fabricate a series of devices with different geometries on the same chip to tailor the electrostatic properties or λ may be amenable to time-dependent tuning within a single device due to a recently proposed tunability of electrostatic circuit capacitances [46] based on quantum geometric effects of the circuit. Note that this principle is distinct from the possibility to tune the quantum capacitance; see, e.g., Ref. [53].

In this Letter, we explore the possibility to embed the QPNC into larger circuits to create Hamiltonians with a nontrivial density of states (DOS) and how to measure the DOS. In particular, our focus is on investigating the role of the parasitic linear capacitive energy term $\sim E_C$, which will prove to be pivotal in spite of being small. All considered model systems can be described by

$$\widehat{H}_d = \widehat{H}_J(\widehat{\varphi}_1, \ldots \widehat{\varphi}_d) + \sum_{j=1}^{d} \widehat{H}^j_{\mathrm{QPNC},} \tag{2}$$

where each $\widehat{H}^j_{\mathrm{QPNC}}$ is given by Eq. (1) after inserting the respective island charge $\widehat{N}_j$. $\widehat{H}_J$ represents a generic Hamiltonian describing a multiterminal junction, connecting $d+1$ superconducting contacts (for an example with $d=2$, see Fig. 1). Explicit junction Hamiltonians are given in the following sections, each about a specific 1D or 2D system. One contact is put to ground, such that its superconducting phase can be fixed to zero. There then remain d islands, each of which is connected with an individual QPNC. The islands' degrees of freedom are the canonically conjugate phase and charge operators $[\widehat{\varphi}_j, \widehat{N}_k] = i\delta_{jk}$.

The charge space spanned by the eigenstates of all $\widehat{N}_j$ can thus be considered as the equivalent of a d-dimensional lattice, where the junction $\widehat{H}_J$ encodes tunneling between lattice points and (optionally) intrinsic degrees of freedom which act as a pseudospin. While the junction energy here corresponds to a kinetic term, the QPNC provides a quasiperiodic potential ($\sim E_S$) on top of a harmonic trap ($\sim E_C$). For simplicity, we assume that E_S and E_C are the same for each island.

Each charge island is subject to an induced offset charge. Note that due to the details of its implementation, the QPNC is affected by two independent sources of offset charges [29] for the quasiperiodic ($\sim E_S$) and for the quadratic term ($\sim E_C$). These independent offset charges are included in Eq. (2) by shifting $\widehat{N}_j \longrightarrow \widehat{N}_j + N^{\alpha}_{g,j}$, where $\alpha = C, S$, respectively. In all the following considerations of the DOS and the numerical computations of such, we consider an averaging over these offset charges.

Our main focus is the analysis of the DOS of $\widehat{H}_d$,

$$\rho(E) = \frac{1}{D}\sum_n \delta(E - \epsilon_n), \tag{3}$$

where ϵ_n are the eigenvalues of $\widehat{H}_d$ and D is the size of the Hilbert space. We hone in on two example systems. We study a 1D system, where the only island is connected to ground with an ordinary Josephson junction, and a 2D system with a Dirac junction, i.e., a three-terminal junction showing a Dirac spectrum [see Fig. 1(a)]. For $E_C = 0$, the 1D system implements the Aubry-André model [54,55] which displays a fractal energy spectrum colloquially known as Hofstadter's butterfly [56]. The 2D system simulates a spin-orbit-coupled tight binding model that hosts Dirac cones [33,57], cf. Eq. (1) below, subject to a quasiperiodic scalar potential. It was recently demonstrated that weak potentials give rise to the same phenomena as the magic angle in twisted bilayer graphene by coupling Dirac particles of different valleys [33,36,47,58]. The phenomenology includes flat and isolated minibands (cf. Fig. 3 below), multiple magic angles, and emergent Dirac excitations on the moiré scale (but Anderson localization at larger values of the potential).

Some general remarks are in order. First, there is a crucial difference between the here-considered circuit implementation, compared to many-body solid state or cold-atomic systems. If the lattice points actually referred to positions of particles, then there would be a meaningful way to extend the description to a many-particle wave function. The charge lattice positions in $\widehat{H}_d$ on the other hand (see Fig. 1) already *are* in second quantized form, as the observables $\widehat{N}_j$ count the number of charges on island j. Therefore, the ground state of $\widehat{H}_d$, ϵ_0, is the many-body ground state and there is no meaningful way to emulate quantities like, e.g., a chemical potential. This is an important and, as a matter of fact, advantageous feature; namely, by means of probing the ac response of a circuit realizing $\widehat{H}_d$, one is capable of directly measuring the DOS that would correspond to the single-particle DOS if $\widehat{H}_d$ referred to positions of a particle instead of the circuit's charge configuration [59]. It is in this sense that we refer to ρ as a single-particle DOS.

The second important remark concerns the role of the parasitic linear capacitances, $\sim E_C$. In the existing literature, the DOS for the above models has been most widely studied in a condensed matter context, where there is no harmonic trapping potential, defining the untrapped model $\widehat{H}_0 \equiv \widehat{H}_d(E_C = 0)$. We here find that while the DOS of $\widehat{H}_0$, $\rho_0(E)$, is related to $\rho(E)$, the connection is nontrivial. In particular, $\rho(E)$ for the system with finite E_C does *not* simply approach $\rho_0(E)$ (the untrapped system) when going to the limit $E_C \to 0$ [60]. This is due to the fact that there is no perturbative limit for the trapping energy as the potential strength diverges sufficiently far away from the origin. Instead, as $E_C \to 0$, we find the convolution formula [48]

$$\rho(E) \approx \int_{E_0}^{E} dE'(E - E')^{\frac{d}{2}-1}\rho_0(E') \overset{d=2}{\to} \partial_E \rho = \rho_0, \tag{4}$$

where E_0 is the bottom of the band. Consequently, the DOS gets distorted in a way characteristic of dimensionality d. For instance, a delta peak in $\rho_0(E)$ morphs either into a van Hove singularity with algebraic tail $\sim 1/\sqrt{E}$ (for $d=1$) or into a Heaviside step function (for $d=2$) in $\rho(E)$. More generally, in $d=1$ peak features survive, whereas in $d=2$ peak features translate into staircaselike features, as reflected in the simple relationship given in the second equality in Eq. (4). We now proceed with numerical calculations [48] of the above introduced explicit models with $d = 1, 2$.

Aubry-André model and Hofstadter's butterfly. We begin by exploring quasiperiodicity in a simple 1D system in conjunction with a harmonic trap [61]. While aspects of this problem have previously been studied with ultracold atoms [62–64] as well as acoustic [65], photonic [66,67], and polaritonic [68] emulators, quantum circuits present another, extremely compact platform, where circuit-specific observables allow a direct measurement of the characteristic Hofstadter DOS.

Consider $\widehat{H}_{d=1}$ from Eq. (2) with the central junction being a simple Josephson junction, $\widehat{H}^{d=1}_J = -E_J\cos(\widehat{\varphi}_1)$ with $E_J = E_S$. For $E_C = 0$, this is the Aubry-André model, which produces the famous HB pattern [56]; see Fig. 2(a). In accordance with Eq. (4), the influence of the finite trapping term

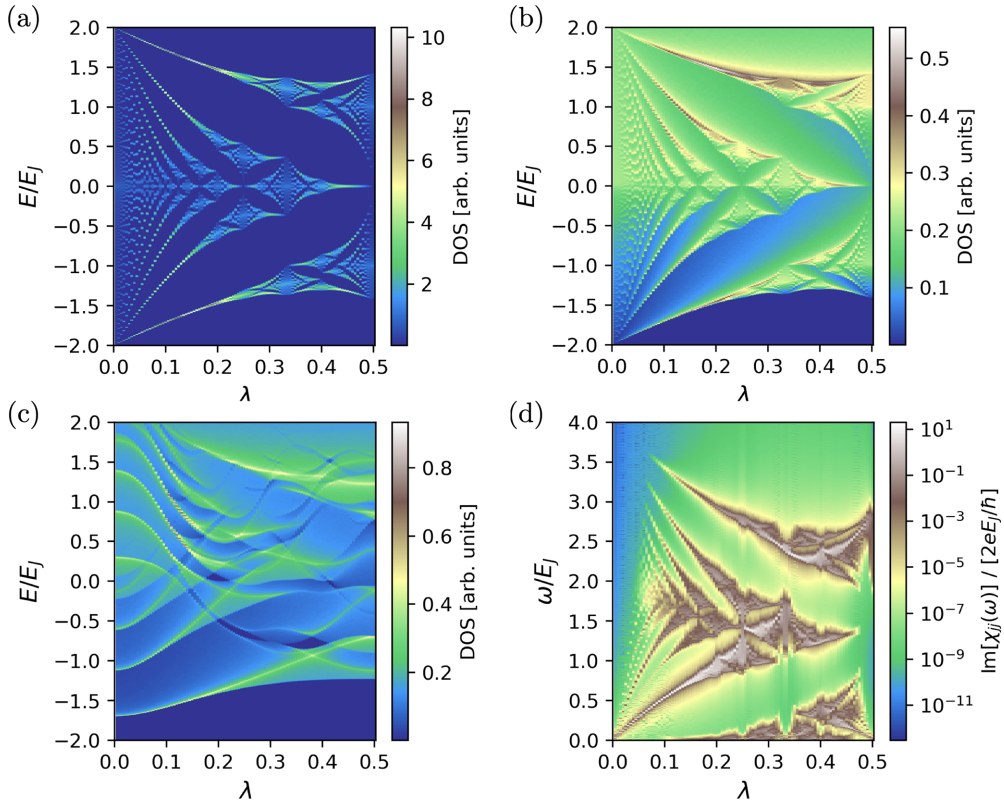

FIG. 2. Spectral functions of Hofstadter butterfly emulator. We consider the 1D system with $E_J = E_S$ for (a) $E_C = 0$ (the original Hofstadter butterfly), (b) $E_C \sim 10^{-4}E_S$, and (c) $E_C = 10^{-1}E_S$. (d) The autocorrelation of the current response on a logarithmic scale with $E_C \sim 10^{-4}E_S$ resembles the density of states shown in (b). The original Hofstadter butterfly (a) was computed in a discretized phase space with 600 lattice points, while for finite E_C the computations were done on a charge lattice of size (b), (d) 271, respectively, (c) 11. The expansion orders of the kernel polynomial method are, respectively, (a) 651; (b), (d) 1474; and (c) 1822.

$E_C \neq 0$ is nontrivial. Energy gaps in the pure HB are now filled with a background density of states due to the already mentioned algebraic tails $\sim 1/\sqrt{E}$; see Figs. 2(b) and 2(c). Nevertheless, for $E_C/E_S \sim 10^{-4}$, Fig. 2(b), the HB is clearly visible in the peaks of the DOS. When going to values close to $E_C/E_S \sim 10^{-1}$, Eq. (4) starts to lose its validity; see Fig. 2(c). Due to the increased harmonic trap, the system gets a larger level spacing and thus the system is no longer in a quasi-continuum limit. Note that $E_C/E_J (= E_C/E_S) \sim 10^{-2}$ corresponds to the regime where transmon devices are typically operated [48].

The DOS of a quantum circuit can be straightforwardly measured via ac spectroscopy in various manners. For theoretical and experimental literature on the light-matter couplings in cQED, we refer the reader to Refs. [69–79]. For concreteness, we here explicitly study a specific measurement of the DOS via a current response due to an external flux, analogously to Ref. [80]. The standard linear response to a time-dependent magnetic flux $\varphi_j \to \varphi_j + \varphi^j_{\rm ext}(t)\theta(t - t_0)$ yields the autocorrelated response function [48]

$$\mathrm{Im}[\chi_{jj}(\omega > 0)] = \pi |\langle \epsilon_0 | \widehat{I}_j | \epsilon_0 + \omega \rangle|^2 \rho(\epsilon_0 + \omega), \qquad (5)$$

with the current operator $\widehat{I}_j = -2e\, i[\widehat{H}_J, \widehat{N}_j]$, eigenenergies ϵ_n, and eigenstates $|\epsilon_n\rangle$. The autocorrelator means that the ac driving and current measurement occur at the same port [81]. We show this response in Fig. 2(d) with a logarithmic color scale in units of $2eE_J/\hbar$. We observe that while the HB pattern still persists, it is distorted with respect to Figs. 2(a)–2(c). This is simply because for the response function the λ-dependent ground state energy is automatically set to zero as a reference point.

Magic-angle effect in 2D Dirac systems. We now move on to consider a three-terminal junction [$d = 2$ in Eq. (2)] with a generic two-dimensional Dirac structure

$$\widehat{H}^D_J = E_{DJ} \begin{pmatrix} 0 & \sin(\widehat{\varphi}_1) + i \sin(\widehat{\varphi}_2) \\ \sin(\widehat{\varphi}_1) - i \sin(\widehat{\varphi}_2) & 0 \end{pmatrix}, \qquad (6)$$

see Fig. 1. Such a Dirac junction can be realized, e.g., with four-terminal Weyl circuits [4,13,14] by closing two contacts by a flux-threaded loop and tuning the external flux to the degeneracy point. While in this construction, the Dirac points would not be topologically protected, residual side effects of a fluctuating minigap due to flux noise could likely be mitigated by increasing the loop area (at the cost of a non-negligible loop inductance in the limit of very large loops). Dirac physics have also been predicted in several other conventional circuits (consisting of regular Josephson junctions), either in a mixed 2D phase-charge space [29] or in a pure charge-charge space [19]. We expect that charge and phase degrees of freedom in these proposals can be swapped by exploiting the duality between Josephson and quantum phase slip junctions [82].

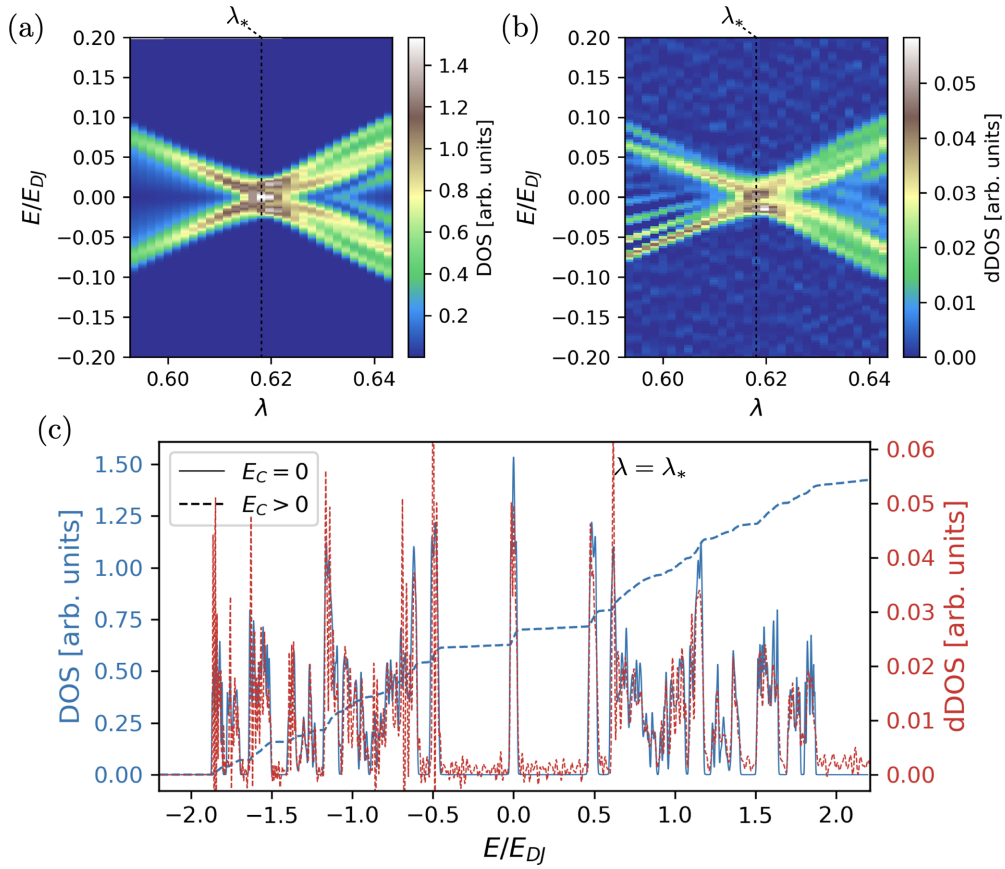

FIG. 3. Spectral signatures of the magic-angle emulator. Here, with $E_S/E_{DJ} = 0.541$ a magic angle appears at $\lambda = \lambda_* \approx 0.62$. (a) The density of states (DOS) for $E_C = 0$ shows the characteristic magic-angle effect. (b) For a finite $E_C \sim 10^{-4}E_{DJ}$, the same characteristic pattern emerges in the differential DOS (dDOS), $\partial_E \rho(E)$. Note that some weakly negative values have been cut to match the color scale of panel (a) [48]. (c) Comparison of the DOS for $E_C/E_{DJ} = 0, 10^{-4}$ (blue solid and blue dashed) and dDOS for $E_C/E_{DJ} = 10^{-4}$ (red dashed), all at $\lambda = \lambda_*$. The DOS for finite E_C has been scaled up by a factor of 40 to allow for direct comparison. All these spectra were computed in a discretized phase space with 610^2 lattice points, while the expansion orders of the kernel polynomial method are, respectively, (a) 1430, (b) 4019, and (c) 1430 ($E_C = 0$) and 4019 ($E_C > 0$).

For $E_C = 0$, it was previously demonstrated [33] that $\widehat{H}^D_{d=2} = \widehat{H}^D_J + \sum_{j=1}^2 \widehat{H}^j_{\mathrm{QPNC}}$ exhibits magic-angle physics in the same universal fashion as twisted bilayer graphene [33,47,83] with the characteristic flat bands [58] and nonzero DOS at zero energy for critical values of E_S and λ; see Fig. 3(a). Consistently with Eq. (4) (and subsequent discussion), we here numerically demonstrate that the same transition can also be observed in the presence of a finite $E_C > 0$. The characteristic magic-angle structure of the DOS now reveals itself in the form of steps surrounded by plateaus of constant DOS (or as peaks in the differential DOS, referred to as dDOS) at the precise values of energy, where the system without trap exhibits flat band peaks; see Figs. 3(b) and 3(c). This result numerically confirms the convolution formula, Eq. (4), for $d = 2$. In analogy with the previous section, one can measure this feature by means of an ac response of the circuit, here, in particular, with a form of differential response $\partial_\omega \chi_{jj}$. Once again, if the device is prepared in the ground state [roughly at $-2E_{DJ}$ in Fig. 3(c)], the magic angle peak will be visible at a driving frequency of $\sim 2E_{DJ}$ [where driving and ac spectroscopy occur as outlined in Eq. (5)]. This finding constitutes one of our main results: the emulation of magic-angle physics in superconducting circuits requiring a relatively small number of conventional circuit elements. Finally, we insist that harmonic traps are a feature transcending the narrow context of superconducting circuits and our specific realization of QPNCs [29], such that the demonstrated survival of the magic-angle feature in the presence of such traps [underlined by Eq. (4)] is expected to also be of importance for many other platforms.

Conclusion and outlook. We demonstrate that conventional circuit elements can reproduce the DOS from a wide variety of solid state moiré materials, such as the Hofstadter butterfly and the magic-angle effect. We show both analytically and numerically that distortions of the DOS due to harmonic traps (parasitic linear capacitances) do not impede the observation of characteristic features—a finding relevant beyond the superconducting circuit context. We further show that straightforward ac current responses directly probe the DOS. Our results prepare the ground for a multitude of future research directions, such as the inclusion of effective many-body features by increasing the number of circuit degrees of freedom. The main challenge for such a generalization is likely the imitation of bosonic (fermionic) exchange statistics,

exactly because the wave function is already embedded in a many-body Hilbert space and as such does not naturally have the required (anti)symmetry in charge space. Another nontrivial extension is to use the circuit-specific flexibility to emulate topological materials with $d > 3$ (see, e.g., Ref. [17] for a junction emulating a topological material with $d = 4$ exhibiting a nonzero second Chern number), and study the so far poorly understood interplay between moiré patterns and topological band structures beyond the usual limitation of three (spatial) dimensions.

Acknowledgments. T.H. and R.P.R. gratefully acknowledge computing time on the supercomputer JURECA [84] at Forschungszentrum Jülich under Grant No. JIFF23. This work has been funded by the German Federal Ministry of Education and Research within the funding program Photonic Research Germany under the Contract No. 13N14891. J.H.P. is partially supported by the Air Force Office of Scientific Research under Grant No. FA9550-20-1-0136 and the Alfred P. Sloan Foundation through a Sloan Research Fellowship. The Flatiron Institute is a division of the Simons Foundation. Support for this research was provided by the Office of the Vice Chancellor for Research and Graduate Education at the University of Wisconsin–Madison with funding from the Wisconsin Alumni Research Foundation. This research was supported in part by Grant No. NSF PHY-2309135 to the Kavli Institute for Theoretical Physics (KITP). E.J.K. and J.H.P. acknowledge hospitality by the KITP.

[1] R. Leone, L. P. Lévy, and P. Lafarge, Cooper-pair pump as a quantized current source, Phys. Rev. Lett. **100**, 117001 (2008).

[2] Leone and Monjou, Merging diabolical points of a superconducting circuit, Condens. Matter Phys. **16**, 33801 (2013).

[3] T. Yokoyama and Y. V. Nazarov, Singularities in the Andreev spectrum of a multiterminal Josephson junction, Phys. Rev. B **92**, 155437 (2015).

[4] R.-P. Riwar, M. Houzet, J. S. Meyer, and Y. V. Nazarov, Multi-terminal Josephson junctions as topological matter, Nat. Commun. **7**, 11167 (2016).

[5] E. Strambini, S. D'Ambrosio, F. Vischi, F. S. Bergeret, Y. V. Nazarov, and F. Giazotto, The ω-squipt as a tool to phase-engineer Josephson topological materials, Nat. Nanotechnol. **11**, 1055 (2016).

[6] E. Eriksson, R.-P. Riwar, M. Houzet, J. S. Meyer, and Y. V. Nazarov, Topological transconductance quantization in a four-terminal Josephson junction, Phys. Rev. B **95**, 075417 (2017).

[7] J. S. Meyer and M. Houzet, Nontrivial Chern numbers in three-terminal Josephson junctions, Phys. Rev. Lett. **119**, 136807 (2017).

[8] H.-Y. Xie, M. G. Vavilov, and A. Levchenko, Topological Andreev bands in three-terminal Josephson junctions, Phys. Rev. B **96**, 161406(R) (2017).

[9] H.-Y. Xie, M. G. Vavilov, and A. Levchenko, Weyl nodes in Andreev spectra of multiterminal Josephson junctions: Chern numbers, conductances, and supercurrents, Phys. Rev. B **97**, 035443 (2018).

[10] O. Deb, K. Sengupta, and D. Sen, Josephson junctions of multiple superconducting wires, Phys. Rev. B **97**, 174518 (2018).

[11] E. V. Repin, Y. Chen, and Y. V. Nazarov, Topological properties of multiterminal superconducting nanostructures: Effect of a continuous spectrum, Phys. Rev. B **99**, 165414 (2019).

[12] E. V. Repin and Y. V. Nazarov, Weyl points in multiterminal hybrid superconductor-semiconductor nanowire devices, Phys. Rev. B **105**, L041405 (2022).

[13] V. Fatemi, A. R. Akhmerov, and L. Bretheau, Weyl Josephson circuits, Phys. Rev. Res. **3**, 013288 (2021).

[14] L. Peyruchat, J. Griesmar, J. D. Pillet, and Ç. Ö. Girit, Transconductance quantization in a topological Josephson tunnel junction circuit, Phys. Rev. Res. **3**, 013289 (2021).

[15] R. L. Klees, G. Rastelli, J. C. Cuevas, and W. Belzig, Microwave spectroscopy reveals the quantum geometric tensor of topological Josephson matter, Phys. Rev. Lett. **124**, 197002 (2020).

[16] R. L. Klees, J. C. Cuevas, W. Belzig, and G. Rastelli, Ground-state quantum geometry in superconductor–quantum dot chains, Phys. Rev. B **103**, 014516 (2021).

[17] H. Weisbrich, R. L. Klees, G. Rastelli, and W. Belzig, Second Chern number and non-Abelian Berry phase in topological superconducting systems, PRX Quantum **2**, 010310 (2021).

[18] H. Weisbrich, M. Bestler, and W. Belzig, Tensor monopoles in superconducting systems, Quantum **5**, 601 (2021).

[19] L. Chirolli and J. E. Moore, Enhanced coherence in superconducting circuits via band engineering, Phys. Rev. Lett. **126**, 187701 (2021).

[20] T. Herrig and R.-P. Riwar, Cooper-pair transistor as a minimal topological quantum circuit, Phys. Rev. Res. **4**, 013038 (2022).

[21] A. Melo, V. Fatemi, and A. R. Akhmerov, Multiplet supercurrent in Josephson tunneling circuits, SciPost Phys. **12**, 017 (2022).

[22] H. Xue, Y. Yang, and B. Zhang, Topological acoustics, Nat. Rev. Mater. **7**, 974 (2022).

[23] C. W. Peterson, W. A. Benalcazar, T. L. Hughes, and G. Bahl, A quantized microwave quadrupole insulator with topologically protected corner states, Nature (London) **555**, 346 (2018).

[24] C. W. Peterson, T. Li, W. A. Benalcazar, T. L. Hughes, and G. Bahl, A fractional corner anomaly reveals higher-order topology, Science **368**, 1114 (2020).

[25] A. J. Kollár, M. Fitzpatrick, and A. A. Houck, Hyperbolic lattices in circuit quantum electrodynamics, Nature (London) **571**, 45 (2019).

[26] I. Bloch, J. Dalibard, and W. Zwerger, Many-body physics with ultracold gases, Rev. Mod. Phys. **80**, 885 (2008).

[27] A. Celi, P. Massignan, J. Ruseckas, N. Goldman, I. B. Spielman, G. Juzeliūnas, and M. Lewenstein, Synthetic gauge fields in synthetic dimensions, Phys. Rev. Lett. **112**, 043001 (2014).

[28] J. Cho, D. G. Angelakis, and S. Bose, Fractional quantum Hall state in coupled cavities, Phys. Rev. Lett. **101**, 246809 (2008).

[29] T. Herrig, J. H. Pixley, E. J. König, and R. P. Riwar, Quasiperiodic circuit quantum electrodynamics, npj Quantum Inf. **9**, 116 (2023).

[30] E. Y. Andrei, D. K. Efetov, P. Jarillo-Herrero, A. H. MacDonald, K. F. Mak, T. Senthil, E. Tutuc, A. Yazdani, and A. F. Young,

The marvels of moiré materials, Nat. Rev. Mater. **6**, 201 (2021).

[31] K. F. Mak and J. Shan, Semiconductor moiré materials, Nat. Nanotechnol. **17**, 686 (2022).

[32] S. Y. F. Zhao, N. Poccia, X. Cui, P. A. Volkov, H. Yoo, R. Engelke, Y. Ronen, R. Zhong, G. Gu, S. Plugge, T. Tummuru, M. Franz, J. H. Pixley, and P. Kim, Emergent interfacial superconductivity between twisted cuprate superconductors, in *The 12th international conference on intrinsic Josephson effect and horizons of superconducting spintronics* (2021), p. 73.

[33] Y. Fu, E. J. König, J. H. Wilson, Y.-Z. Chou, and J. H. Pixley, Magic-angle semimetals, npj Quantum Mater. **5**, 71 (2020).

[34] J. Cano, S. Fang, J. H. Pixley, and J. H. Wilson, Moiré superlattice on the surface of a topological insulator, Phys. Rev. B **103**, 155157 (2021).

[35] Sayed Ali Akbar Ghorashi, A. Dunbrack, A. Abouelkomsan, J. Sun, X. Du, and J. Cano, Topological and stacked flat bands in bilayer graphene with a superlattice potential, Phys. Rev. Lett. **130**, 196201 (2023).

[36] Y.-Z. Chou, Y. Fu, J. H. Wilson, E. J. König, and J. H. Pixley, Magic-angle semimetals with chiral symmetry, Phys. Rev. B **101**, 235121 (2020).

[37] T. Salamon, A. Celi, R. W. Chhajlany, I. Frérot, M. Lewenstein, L. Tarruell, and D. Rakshit, Simulating twistronics without a twist, Phys. Rev. Lett. **125**, 030504 (2020).

[38] P. Wang, Y. Zheng, X. Chen, C. Huang, Y. V. Kartashov, L. Torner, V. V. Konotop, and F. Ye, Localization and delocalization of light in photonic moiré lattices, Nature (London) **577**, 42 (2020).

[39] D. Mao and T. Senthil, Quasiperiodicity, band topology, and moiré graphene, Phys. Rev. B **103**, 115110 (2021).

[40] Z. Meng, L. Wang, W. Han, F. Liu, K. Wen, C. Gao, P. Wang, C. Chin, and J. Zhang, Atomic Bose–Einstein condensate in twisted-bilayer optical lattices, Nature (London) **615**, 231 (2023).

[41] J. Lee and J. H. Pixley, Emulating twisted double bilayer graphene with a multiorbital optical lattice, SciPost Phys. **13**, 033 (2022).

[42] S. J. Ahn, P. Moon, T.-H. Kim, H.-W. Kim, H.-C. Shin, E. H. Kim, H. W. Cha, S.-J. Kahng, P. Kim, M. Koshino, Y.-W. Son, C.-W. Yang, and J. R. Ahn, Dirac electrons in a dodecagonal graphene quasicrystal, Science **361**, 782 (2018).

[43] A. Uri, S. C. de la Barrera, M. T. Randeria, D. Rodan-Legrain, T. Devakul, P. J. D. Crowley, N. Paul, K. Watanabe, T. Taniguchi, R. Lifshitz, L. Fu, R. C. Ashoori, and P. Jarillo-Herrero, Superconductivity and strong interactions in a tunable moiré quasicrystal, Nature (London) **620**, 762 (2023).

[44] A. M. Bozkurt, J. Brookman, V. Fatemi, and A. R. Akhmerov, Double-Fourier engineering of Josephson energy-phase relationships applied to diodes, SciPost Phys. **15**, 204 (2023).

[45] W. C. Smith, M. Villiers, A. Marquet, J. Palomo, M. R. Delbecq, T. Kontos, P. Campagne-Ibarcq, B. Douçot, and Z. Leghtas, Magnifying quantum phase fluctuations with Cooper-pair pairing, Phys. Rev. X **12**, 021002 (2022).

[46] R.-P. Riwar, Discrete control of capacitance in quantum circuits, arXiv:2306.00587.

[47] M. Gonçalves, H. Z. Olyaei, B. Amorim, R. Mondaini, P. Ribeiro, and E. V. Castro, Incommensurability-induced subballistic narrow-band-states in twisted bilayer graphene, 2D Mater. **9**, 011001 (2022).

[48] See Supplemental Material at http://link.aps.org/supplemental/10.1103/PhysRevB.111.L201104 for a plot of the Hofstadter-butterfly emulator in the typical transmon regime, a discussion on the quasiperiodic capacitance, details on the numerical methods and the autocorrelated linear response function, and the derivation of the convolution formula on the density of states at finite trapping potential. This includes a reference to A. Weiße, G. Wellein, A. Alvermann, and H. Fehske, The kernel polynomial method, Rev. Mod. Phys. 78, 275 (2006).

[49] J. Koch, T. M. Yu, J. Gambetta, A. A. Houck, D. I. Schuster, J. Majer, A. Blais, M. H. Devoret, S. M. Girvin, and R. J. Schoelkopf, Charge-insensitive qubit design derived from the Cooper pair box, Phys. Rev. A **76**, 042319 (2007).

[50] W. A. Little, Possibility of synthesizing an organic superconductor, Phys. Rev. **134**, A1416 (1964).

[51] A. Hamo, A. Benyamini, I. Shapir, I. Khivrich, J. Waissman, K. Kaasbjerg, Y. Oreg, F. von Oppen, and S. Ilani, Electron attraction mediated by Coulomb repulsion, Nature (London) **535**, 395 (2016).

[52] B. A. Placke, T. Pluecker, J. Splettstoesser, and M. R. Wegewijs, Attractive and driven interactions in quantum dots: Mechanisms for geometric pumping, Phys. Rev. B **98**, 085307 (2018).

[53] T. Duty, G. Johansson, K. Bladh, D. Gunnarsson, C. Wilson, and P. Delsing, Observation of quantum capacitance in the Cooper-pair transistor, Phys. Rev. Lett. **95**, 206807 (2005).

[54] S. Aubry and G. Andre, Analyticity breaking and Anderson localization in incommensurate lattices, Ann. Israel Phys. Soc. **3**, 133 (1980).

[55] P. G. Harper, Single band motion of conduction electrons in a uniform magnetic field, Proc. Phys. Soc. A **68**, 874 (1955).

[56] D. R. Hofstadter, Energy levels and wave functions of Bloch electrons in rational and irrational magnetic fields, Phys. Rev. B **14**, 2239 (1976).

[57] I. Affleck and J. B. Marston, Large-n limit of the Heisenberg-Hubbard model: Implications for high-T_c superconductors, Phys. Rev. B **37**, 3774 (1988).

[58] J. Yi, E. J. König, and J. H. Pixley, Low energy excitation spectrum of magic-angle semimetals, Phys. Rev. B **106**, 195123 (2022).

[59] As already hinted at in the Introduction, an ac driving of solid state systems or cold atom gases would, in general, generate a more complicated response involving many-body excitations and interactions.

[60] While E_C can be tuned to very small values (see Ref. [29]), it is practically impossible, respectively, physically meaningless, to have exactly zero charging energy $E_C = 0$.

[61] M. Modugno, Exponential localization in one-dimensional quasi-periodic optical lattices, New J. Phys. **11**, 033023 (2009).

[62] G. Roati, C. D'Errico, L. Fallani, M. Fattori, C. Fort, M. Zaccanti, G. Modugno, M. Modugno, and M. Inguscio, Anderson localization of a non-interacting Bose–Einstein condensate, Nature (London) **453**, 895 (2008).

[63] H. P. Lüschen, S. Scherg, T. Kohlert, M. Schreiber, P. Bordia, X. Li, S. Das Sarma, and I. Bloch, Single-particle mobility edge in a one-dimensional quasiperiodic optical lattice, Phys. Rev. Lett. **120**, 160404 (2018).

[64] Y. Wang, J.-H. Zhang, Y. Li, J. Wu, W. Liu, F. Mei, Y. Hu, L. Xiao, J. Ma, C. Chin, and S. Jia, Observation of interaction-induced mobility edge in an atomic Aubry-André wire, Phys. Rev. Lett. **129**, 103401 (2022).

[65] X. Ni, K. Chen, M. Weiner, D. J. Apigo, C. Prodan, A. Alu, E. Prodan, and A. B. Khanikaev, Observation of Hofstadter butterfly and topological edge states in reconfigurable quasi-periodic acoustic crystals, Commun. Phys. **2**, 55 (2019).

[66] Y. Lahini, R. Pugatch, F. Pozzi, M. Sorel, R. Morandotti, N. Davidson, and Y. Silberberg, Observation of a localization transition in quasiperiodic photonic lattices, Phys. Rev. Lett. **103**, 013901 (2009).

[67] Y. E. Kraus, Y. Lahini, Z. Ringel, M. Verbin, and O. Zilberberg, Topological states and adiabatic pumping in quasicrystals, Phys. Rev. Lett. **109**, 106402 (2012).

[68] V. Goblot, A. Štrkalj, N. Pernet, J. L. Lado, C. Dorow, A. Lemaître, L. Le Gratiet, A. Harouri, I. Sagnes, S. Ravets *et al.*, Emergence of criticality through a cascade of delocalization transitions in quasiperiodic chains, Nat. Phys. **16**, 832 (2020).

[69] A. Blais, A. L. Grimsmo, S. M. Girvin, and A. Wallraff, Circuit quantum electrodynamics, Rev. Mod. Phys. **93**, 025005 (2021).

[70] M. Fuechsle, J. Bentner, D. A. Ryndyk, M. Reinwald, W. Wegscheider, and C. Strunk, Effect of microwaves on the current-phase relation of superconductor–normal-metal–superconductor Josephson junctions, Phys. Rev. Lett. **102**, 127001 (2009).

[71] L. Bretheau, Ç. Ö. Girit, H. Pothier, D. Esteve, and C. Urbina, Exciting Andreev pairs in a superconducting atomic contact, Nature (London) **499**, 312 (2013).

[72] L. Bretheau, Ç. Ö. Girit, C. Urbina, D. Esteve, and H. Pothier, Supercurrent spectroscopy of Andreev states, Phys. Rev. X **3**, 041034 (2013).

[73] S. Novikov, J. E. Robinson, Z. K. Keane, B. Suri, F. C. Wellstood, and B. S. Palmer, Autler-Townes splitting in a three-dimensional transmon superconducting qubit, Phys. Rev. B **88**, 060503(R) (2013).

[74] D. J. van Woerkom, A. Proutski, B. van Heck, D. Bouman, J. I. Väyrynen, L. I. Glazman, P. Krogstrup, J. Nygård, L. P. Kouwenhoven, and A. Geresdi, Microwave spectroscopy of spinful Andreev bound states in ballistic semiconductor Josephson junctions, Nat. Phys. **13**, 876 (2017).

[75] K. V. Shulga, P. Yang, G. P. Fedorov, M. V. Fistul, M. Weides, and A. V. Ustinov, Observation of a collective mode of an array of transmon qubits, JETP Lett. **105**, 47 (2017).

[76] A. Proutski, D. Laroche, B. van 't Hooft, P. Krogstrup, J. Nygård, L. P. Kouwenhoven, and A. Geresdi, Broadband microwave spectroscopy of semiconductor nanowire-based Cooper-pair transistors, Phys. Rev. B **99**, 220504(R) (2019).

[77] L. Tosi, C. Metzger, M. F. Goffman, C. Urbina, H. Pothier, S. Park, A. L. Yeyati, J. Nygård, and P. Krogstrup, Spin-orbit splitting of Andreev states revealed by microwave spectroscopy, Phys. Rev. X **9**, 011010 (2019).

[78] A. Bargerbos, M. Pita-Vidal, R. Žitko, J. Ávila, L. J. Splitthoff, L. Grünhaupt, J. J. Wesdorp, C. K. Andersen, Y. Liu, L. P. Kouwenhoven, R. Aguado, A. Kou, and B. van Heck, Singlet-doublet transitions of a quantum dot Josephson junction detected in a transmon circuit, PRX Quantum **3**, 030311 (2022).

[79] D. Willsch, D. Rieger, P. Winkel, M. Willsch, C. Dickel, J. Krause, Y. Ando, R. Lescanne, Z. Leghtas, N. T. Bronn, P. Deb, O. Lanes, Z. K. Minev, B. Dennig, S. Geisert, S. Günzler, S. Ihssen, P. Paluch, T. Reisinger, R. Hanna *et al.*, Observation of Josephson harmonics in tunnel junctions, Nat. Phys. **20**, 815 (2024).

[80] F. Kos, S. E. Nigg, and L. I. Glazman, Frequency-dependent admittance of a short superconducting weak link, Phys. Rev. B **87**, 174521 (2013).

[81] Note that it is by all means possible to consider cross-correlators where driving and measurement are performed at different ports. All types of correlators will depend on the same DOS such that these details do not matter.

[82] J. Ulrich and F. Hassler, Dual approach to circuit quantization using loop charges, Phys. Rev. B **94**, 094505 (2016).

[83] R. Bistritzer and A. H. MacDonald, Moiré bands in twisted double-layer graphene, Proc. Natl. Acad. Sci. USA **108**, 12233 (2011).

[84] Jülich Supercomputing Centre, JURECA: Data Centric and Booster Modules implementing the Modular Supercomputing Architecture at Jülich Supercomputing Centre, J. Large Scale Res. Facil. **7**, A182 (2021).